Segmentation and assessment of structural plasticity of hippocampal dendritic spines from 3D confocal light microscopy

Subhadip Basu*[a], Punam Kumar Saha[b], Ewa Baczynska[c], Matylda Roszkowska[c], Marta Magnowska[c], Nirmal Das[a], Indranil Guha[b], Jakub Wlodarczyk*[c]
[a]Department of Computer Science and Engineering, Jadavpur University, Kolkata, 700032, India.;
[b]Department of Electrical and Computer Engineering and Department of Radiology, University of Iowa, Iowa City, IA 52242, USA.;
[c]Nencki Institute of Experimental Biology, Polish Academy of Sciences, Pasteura 3, Warsaw, 02-093, Poland.

ABSTRACT

We present new methods for segmentation of hippocampal dendritic spines in 3D confocal light microscopy and computation of 3-D morphological attributes characterizing dendritic spine plasticity. The methods are applied on 3D confocal light microscopy images of dendritic spines from dissociated hippocampal cultures. The segmentation method is based on the principle of multi-scale opening which uses a set of user-specified seeds and iteratively segments structures at different scales starting at a large scale and progressing toward finer scales. The accuracy of the segmentation method is evaluated by comparing its results with the gold standard obtained by manual labelling. The reproducibility of the overall method involving segmentation as well as computation of structural measures is assessed by comparing the values of structural measures derived from segmentation results generated using seeds from three mutually-blinded users. Finally, the performance of the overall method is examined in terms of its ability to characterize spine morphological changes after chemically induced long-term potentiation.

Keywords: Confocal microscopy, Multiscale opening, Plasticity, Dendritic spines, Spine Morphology

1. INTRODUCTION

Dendrites of different neurons in different regions of the brain are covered with a small membranous protrusions called dendritic spine [1] that receives excitatory input from a single axon at the synapse [2]. The dendrites of a single neuron can have of hundreds to thousands of spines. The dendrites of a single neuron can have of hundreds to thousands of spines. Dendritic spines are of distinct structural features and fall in a heterogeneous group in terms of size and shape. Morphologically, dendritic spines have two parts one is a spine head and another is a thin neck which connects the spine to the parent dendrite [3]. Dendritic spines are essential for the accurate activity and signal transmission of neural circuits, but their exact function is still hard to understand and remains under comprehensive research [456]. The shape of dendritic spines may change depending on activity- and experience which link synaptic plasticity [7891011] with biological phenomena that are critical for synaptic function [1213]. Although the consequences of these morphological changes are not clear, many researchers believe structural plasticity of dendritic spines assist learning and memory [6]. According to [14] the structural plasticity of dendritic spines is indeed related to synaptic function. Recent works propose the structural models of synaptic plasticity which links long-term potentiation with spine enlargement [1516].

Due to complex morphology of the dendritic spines, many aspects of the existing relation between structure and synaptic function is unknown [1718]. Although significant progress have been made in imaging technologies for both *in vivo* and *in vitro*, the limited optical resolution of images obtained using popular confocal microscopy technique lead to difficulties in spine segmentation from dendrites and the identification of true spine boundaries [192021]. Therefore, the accurate quantitative analysis of spines is a challenge to the neuroscientists. A robust and unbiased image analysis tool for quantitative analysis of dendritic spine morphology is need of the time [2223].

The most popular approach to address the issue is using two-dimensional (2-D) images that are generated from the maximum intensity projection (MIP) of the image stack, acquired by high-resolution confocal microscopy. A PCT application [24] presents a method for characterizing one or more neurons and dendritic spines using a grassfire process but the detailed description of precise spine contour detection is missing. A US patent application [25] presents a method for

determining neuronal morphology and the effects of substances thereon using dendritic spine detection. The work [2627] presents a method for the segmentation and analysis of every spine separately using a contour tracing algorithm to detect the spine boundary and morphological attributes. However, the spine segmentation process requires extensive user intervention and is time-consuming and error-prone. Basu et al. [28] recently published a more accurate and rapid tool for assessing spine features from 2-D MIP images of dendritic spines. Authors used a novel convolution kernel-based approach to segment the spines from the dendritic segments and classified the segmented spines into one of four categories: stubby, filopodia, mushroom, and spine-head protrusions.

However, all of these methods utilize 2-D MIP images of dendritic spines to analyze structural details of individual spines. Accurate analysis is nearly impossible based on 2-D MIP images of dendritic spines because MIP images are highly discontinuous and may lead to erroneous analysis. Therefore, in the present work, we focused on analyzing dendritic spine images based on 3-D volume that were generated from the confocal image stack. A few previous studies also addressed the issue of individual spine morphometry. Imaris software [29] is a commercially available tool for the four-dimensional (4-D) analysis of dendritic spines. Although Imaris software is good for analyzing the overall spine population, it fails to accurately model the three-dimensional (3-D) morphology of individual spines. Swanger et al. [30] also reported an automated method for the 4-D analysis of dendritic spine morphology using the same Imaris pipeline. Both methods generally fail to assess individual spine plasticity.

In the present study, different neurons from rat dissociated hippocampal cultures were imaged using a confocal light microscope after chemically induced long-term potentiation (cLTP). The methodology that we developed allows the user to mark specific dendritic spines and uses a multi-scale opening (MSO) algorithm [313233] to segment the spines as 3-D volumes, and extract relevant morphometric features with high accuracy and minimal user intervention for the accurate assessment of dendritic spine plasticity. We mathematically defined different key spine compartments (e.g., spine head and spine neck) and observed the changes of their morphological attributes (e.g., Total Volume, spine length, and head width) with cLTP. However, the accurate quantification of structural changes was perceived to be difficult because of the insufficient spatial resolution of confocal microscopy. Our experimental observations showed that cLTP led to coordinated morphological changes in total spine volume, spine length, spine necks and head width. We validated the feasibility of accurately analyzing dendritic spines morphologically using confocal microscopy despite its limited spatial resolution.

2. THEORY AND METHODS

In this work [32] we have used the concept of the MSO algorithm for the segmentation task. MSO algorithm combines the concept of fuzzy distance transform (FDT) [34], iterative fuzzy connectivity (IFC) [3536] and and iterative relative fuzzy connectivity (IRFC) [3738]. The concept of FDT, FC and IRFC has been widely used in many image processing tasks [3940] before. The MSO algorithm gradually erode the assembly of two fused objects, in this case spines and dendrites, until those two objects become mutually disconnected, thus creating two separate objects. The first iteration starts with two sets of seed voxels, S_{Spine} and S_{Dendrite}, and a set of common separators, S_S. The initial FDT map $\Omega_{\text{Spine},0}$ for the first object is computed from the combined image space, except that the voxels in $S_{\text{Dendrite}} \cup S_S$ are added to the background. The FDT map $\Omega_{\text{Dendrite},0}$ for the other object is computed similarly. The sets S_{Spine}, S_{Dendrite}, and S_S are mutually exclusive.

Let us now consider the coupling of two objects with significant intensity overlap, are fused with each other at different unknown locations and scales. Let μ_{Dendrite} and μ_{Spine} denote the dendrite and spine membership functions, defined as the following:

$$\mu_{\text{Dendrite}}(p) = \begin{cases} 0, & \text{if } I(p) < I_{\text{Spine}}, \\ \frac{I(\text{p}) - I_{\text{Spine}}}{I_{\text{Dendrite}} - I_{\text{Spine}}}, & \text{if } I_{\text{Spine}} \le I(p) < I_{\text{Dendrite}}, \\ 1 & \text{otherwise}, \end{cases} \quad (1)$$

$$\mu_{\text{Spine}}(p) = \begin{cases} 0, & \text{if } I(p) < I_{\min}, \\ 1, & \text{if } I_{\min} \le I(p) < I_{\text{Spine}}, \\ \frac{I_{\text{Dendrite}} - I(p)}{I_{\text{Dendrite}} - I_{\text{Spine}}}, & \text{if } I_{\text{Spine}} \le I(p) < I_{\text{Dendrite}}, \\ 0, & \text{if } I(p) \ge I_{\text{Dendrite}}, \end{cases} \quad (2)$$

where $I: O \to [I_{\min}, I_{\max}]$ is the image intensity function over O, the set of all voxels with non-zero membership. I_{Spine},

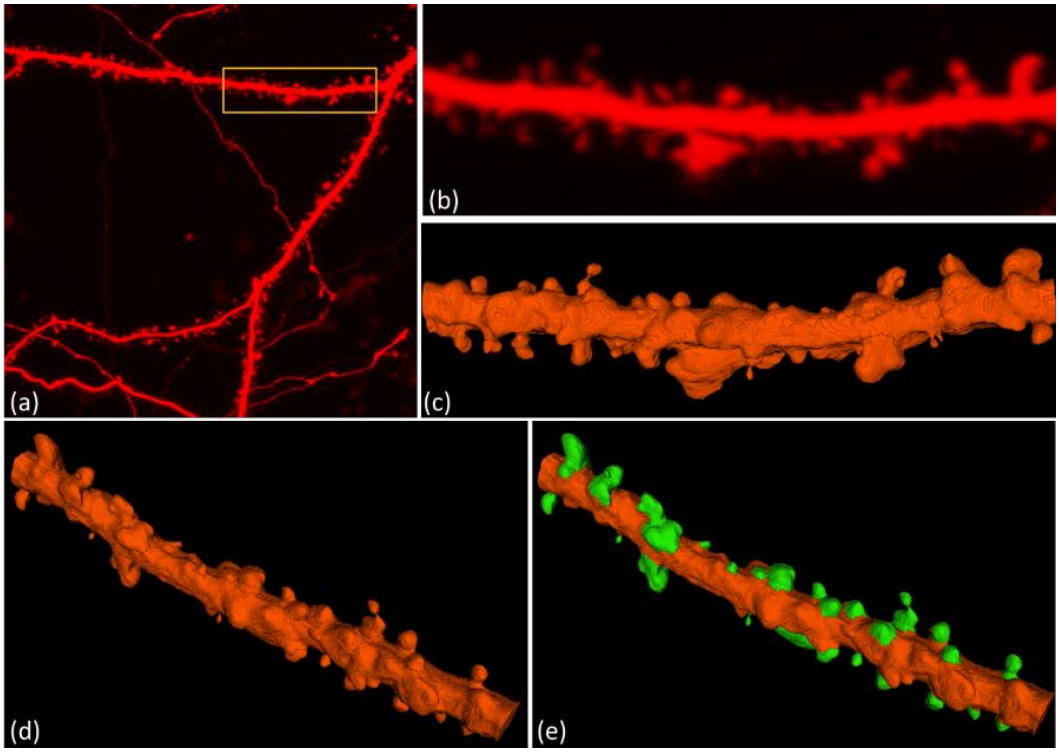

Figure 1. Confocal light microscopy image of hippocampal dendritic spines; a) maximum intensity projection (MIP) of the z-stack with an outlined region-or-interest (ROI), b) the cropped and enlarged MIP image of the selected ROI, c) 3-D rendition of the selected ROI from the confocal z-stack with enhanced morphological details of individual spines, d) reoriented image (c), e) 3-D segmentation result of the selected ROI with the extracted spines marked in green colour.

and I_{Dendrite} is the representative spine and dendrite intensities that define the respective transition between pure and shared intensity bands. Let $P_{\text{Dendrite}} \subset O$ and $P_{\text{Spine}} \subset O$ be the set of voxels that fall inside the pure intensity band for dendrite and spine respectively. Thus, the set of voxels that fall within the shared intensity band is $O_{\text{Shared}} = O - P_{\text{Dendrite}} - P_{\text{Spine}}$. A fuzzy representation of the composite object may be obtained by taking the fuzzy union of the two membership functions that are shown in Equations 1 and 2. The iterative approach of the multi-scale opening of two structures takes several iterations to grow the path-continuity of an object, starting from its seed voxels (commonly added in large-scale regions), to a peripheral location with fine-scale details.

Note that after the iterative propagation of the MSO algorithm, the dendrite region is segmented as a single connected component. O_{Spine} represents one or more disjointed spine regions (R_i), such that $O_{\text{Spine}} = \bigcup_{i=1}^{K} R_i$, where K is the total number of disjointed spine segments in O_{Spine}, and each such segmented spine region R_i contains at least one spine seed $p \in S_{\text{Spine}}$.

Morphological definitions for the spine regions:
After the proper segmentation of dendritic spines, the next task is to mathematically define various spine attributes for assessment of their morphometry. In the present study, we defined several key morphological features of 3-D dendritic spines for plasticity analysis. Specifically, we defined four key spine features that are related to the base and head of a spine using standard notations of digital topology and geometry [4142].

Definition 1. For a given spine $R_i \subset O_{\text{Spine}}$, the *base* of the spine is defined as the set of points $B_i \subset O_{\text{Dendrite}}$ such that $\forall p \in B_i, \exists q \in R_i$ is adjacent to p.

Definition 2. For a given spine $R_i \subset O_{\text{Spine}}$, the *central base point* CBP_i is the centroid of the base of the spine R_i (i.e., $CBP_i = \frac{1}{|B_i|}\sum_{\forall p \in B_i} p$, where $|\cdot|$ is the cardinality of a set).

The head and tip of a spine are defined using the FDT map [34] Ω_i of R_i. A locally deepest point in a spine R_i is a point $p \in R_i$ such that $\forall q \in \mathcal{N}_l(p)\ \Omega_i(q) \leq \Omega_i(p)$, where $\mathcal{N}_l(p)$ is the $(2l+1)^3$ neighborhood of p. Here, $l = 2$ is used to avoid noisy local maxima.

Definition 3. The *center of the head* CH_i of a spine R_i is the locally deepest point in the spine. In a situation where multiple locally deepest points satisfy the farthest distance criterion, their centroid is used.

Definition 4. The *tip of a spine* T_i of a spine R_i is a point $T_i \in R_i$ that is farthest from its central base point CBP_i. In a situation where multiple points of R_i satisfy the farthest distance criterion, their centroid is used.

Note that CBP_i, CH_i, and T_i play key roles in estimating spine attributes, such as *length of the spine*, *neck-length*, *neck-width*, *head-width*, etc., for each individual spine R_i. To estimate these features, we further extended the above definitions to find the geodesic path from *base to head* BH_i of the spine R_i by joining the two central points CBP_i and CH_i such that $\sum_{\forall p \in BH_i} \Omega_i(p)$ is minimized. Likewise, we computed the central path from *head to spine-tip* HT_i of the spine R_i by joining CH_i and T_i, such that $\sum_{\forall p \in HT_i} \Omega_i(p)$ is minimized. Figure 3 shows an illustration of these key spine attributes with respect to a segmented spine.

We now estimate the *neck length* NL_i of R_i as $NL_i = BH_i - \Omega_i(CH_i)$. *Minimum neck-width* MNW_i of R_i is estimated as $MNW_i = \min_{\forall p \in BH_i}(\Omega_i(p))$. *Average head-width* AHW_i of the spine R_i is estimated as $AHW_i = \operatorname{avg}_{\forall p \in HP_i}(\Omega_i(p))$ such that HP_i is the set of all locally deepest points in R_i. Finally, the *length of the spine* L_i is estimated as $L_i = |BH_i| + |HT_i|$.

3. RESULTS

The methodology that we developed is useful in the accurate volumetric assessment of spine plasticity. Two specific challenges are involved in this process: (1) accurate 3-D segmentation of individual spines from the dendritic segment (see Figure 1) and (2) quantitative analysis of individual spine morphology for the assessment of structural changes in dendritic spines (see Figure 2). The confocal light microscopy images of dendritic spines from dissociated hippocampal cultures were used for (1) the analysis of accuracy relative to ground-truth, generated by experimental biologists and the available state-of-the-art Imaris tool, 2) the analysis of reproducibility of the segmentation results, and (3) the quantitative analysis of morphological changes in spines. The detail description of the datasets is given on [28]. In the first dataset, three different neurons from rat dissociated hippocampal cultures were imaged using a confocal light microscope, before and after cLTP(50 μM forskolin, 50 μM picrotoxin, and 0.1 μM rolipram; each dissolved in dimethylsulfoxide [DMSO]) induction. All of the images were captured three times: at baseline (before cLTP) and 10 and 40 min after cLTP induction. In the second dataset, three different neurons from rat dissociated hippocampal cultures were similarly imaged at baseline and 10 and 40 min after mock cLTP induction (i.e., only the solvent, DMSO, was used). During image pre-processing, we took the confocal z-stack and performed Gaussian de-noising on the 3-D image stack. The pre-processed images at time 0 are labeled as T0, and the images that were captured at 10 and 40 min are labeled as T10 and T40, respectively.

Figure 3 shows the segmented spine on a sample dendritic segment. For accuracy analysis, we first generated ground-truth spine segmentation results for all of the neuronal images by manually labeling ideal spine regions of a sample spine population with the help of experimental biologists using the open-source image processing software Fiji [43] and ITK Snap [44]. Although both Fiji and ITK Snap are general-purpose image analysis tools, neither of them are capable of extracting morphological attributes that are specific to a dendritic spine. The 3-D rendering of a sample dendritic segment is shown in Figure 4(a). Manual ground-truth segmentation results of the sample spines are shown in Figure 4(b). For the quantitative analysis of spine segmentation accuracy, we considered the most generic features, such as the volume and length of a spine. We calculated Pearson's correlation coefficients to assess the mean agreement of the estimated feature values between the currently developed method and the ground-truth annotations. The respective Pearson's correlation coefficients for volume and length, estimated over a sample spine population with manually annotated ground-truth results, were 0.89 and 0.82, respectively. For qualitative comparisons of the 3-D segmentation results, we considered the state-of-

the-art Imaris tool [45] that was applied over the same set of images that were considered in this study. Figure 5 shows the qualitative comparisons of our segmentation results with Imaris. In this section, we present multi-user reproducibility of the currently developed method to assess the reliability and robustness of the segmentation methodology. The reproducibility analysis was performed on a sample spine population with three mutually blinded, independent experimental biologists. The percent standard deviations relative to the mean feature estimation for the three independent users were ±16% and ±6% for total volume and spine length, respectively.

For qualitative and quantitative analyses of dendritic spines, we assessed the segmentation results of the currently developed methodology over the same dendritic segments from different sets of the T0, T10, and T40 images. We present detailed 3-D morphological changes in dendritic spines over time (i.e., before and after cLTP). To investigate the relative changes in various morphological attributes of the segmented spines, three important features i.e., total volume, spine length, and head-width were considered from the overall experiment. Figure 6 shows the percent relative changes in these three attributes 10 and 40 min after cLTP induction.

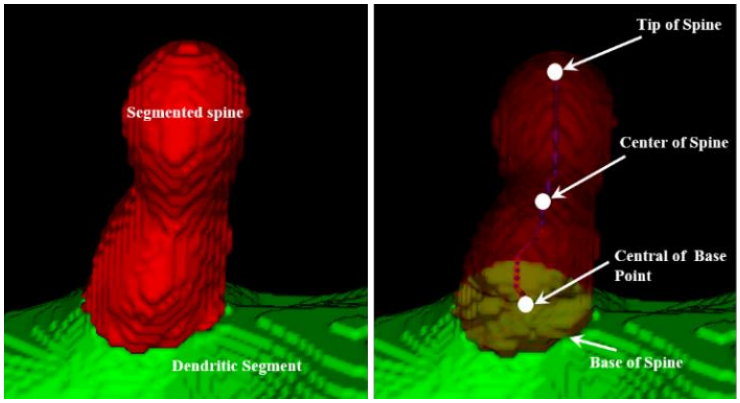

Figure 2. Illustration of a segmented spine structure with automatic quantitative assessment of different spine attributes.

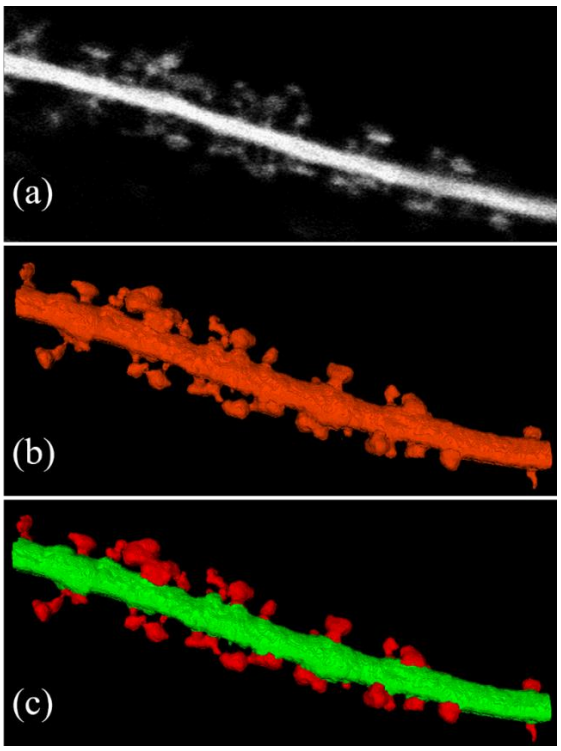

Figure 3. (a) Sample enlarged dendritic segment taken from MIP image of confocal Z stack. (b) 3D rendering of the reconstructed dendritic segment. (c) 3D rendering of the reconstructed dendritic segment with segmented spine shown in red color

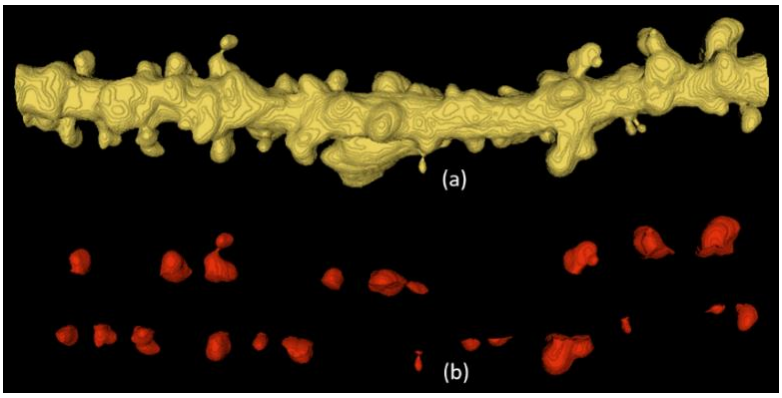

Figure 4. Ground-truth spine segmentation. (a) 3-D rendering of a sample dendritic spine segment. (b) Manual segmentation of the spines obtained from (a) using ITK Snap and Fiji 3-D image processing tools.

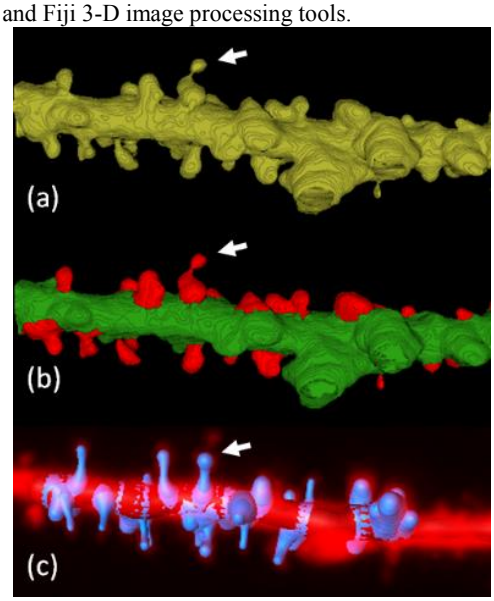

Figure 5. Comparative analysis of 3-D segmentation results relative to the state-of-the-art Imaris tool[45]. The arrows indicate representative spines. (a) 3-D rendering of a spine segment. (b) 3-D segmentation result using the currently developed algorithm. (c) 3-D segmentation result of the same dendritic segment superimposed on the corresponding MIP image.

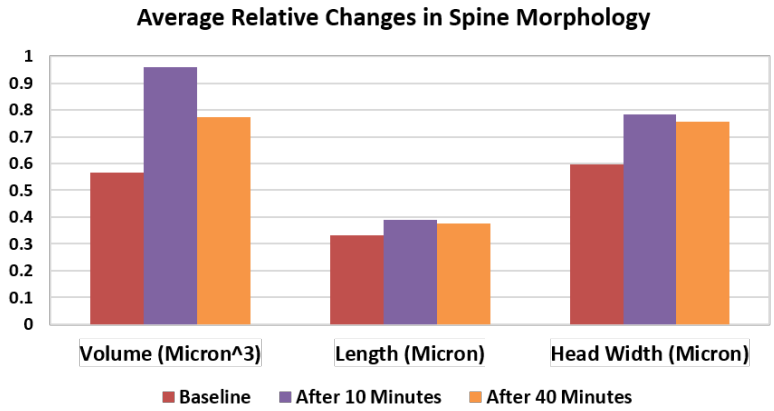

Figure 6. Qualitative percent relative changes in individual spine morphology (Volume, Spine Length and Head Width) estimated by the currently developed method after cLTP induction.

4. CONCLUSION AND DISCUSSION

The present study presented an important issue of accurate 3D segmentation of dendritic spines and qualitative and quantitative assessment of changes in dendritic spine morphology over time. The proposed segmentation method was validated for individual spines using real-time experiments and consecutive images of the same dendritic fragment. Our results are consistent with other studies that reported growth of spine morphological attributes upon cLTP induction [4647]. The plasticity analysis was performed 10 and 40 min after cLTP induction relative to baseline images. Accuracy was evaluated relative to manually labeled ground-truth annotations and segmentation result of state of the art Imaris Tool [45]. To assess the reproducibility of the segmentation results, three blinded experts separately assessed the efficacy of the methodology. The currently developed method was also able to quantitatively assess changes in morphology after cLTP. Although this experiment exclusively used confocal light microscopy images of dendritic spines, the method may be extended in the future for use with other super-high-resolution imaging techniques, such as photo-activated localization microscopy. The present 3-D segmentation method may be used for different experimental protocols that study the structural dynamics of dendritic spines in vitro and in vivo under various physiological and pathological conditions. Moreover, we believe that this will be an excellent research tool that enables the detection of even subtle changes in the 3-D dendritic spine structure. Such methodological advances in spine morphological studies will allow more precise analyses and better interpretations of biological data regarding structural plasticity.

ACKNOWLEDGEMENTS

This project is partially supported by the CMATER research laboratory of the Computer Science and Engineering Department, Jadavpur University, India; UPE-II project and Research Award (F.30-31/2016(SA-II)) from UGC, Government of India, and DBT project (No. BT/PR16356/BID/7/596/2016), Ministry of Science and Technology, Government of India.

REFERENCES

[1] Ramón, S. and Cajal, J., "Textura del sistema nervioso del hombre y de los vertebrados," Rev. Española Patol., 583–584 (2002).

[2] Bourne, J. N. and Harris, K. M., "Balancing Structure and Function at Hippocampal Dendritic Spines," Annu. Rev. Neurosci. **31**(1), 47–67 (2008).

[3] Harris, K. M. and Kater, S. B., "Dendritic Spines: Cellular Specializations Imparting Both Stability and Flexibility to Synaptic Function," Annu. Rev. Neurosci. **17**(1), 341–371 (1994).

[4] Shepherd, G. M., "The dendritic spine: a multifunctional integrative unit," J. Neurophysiol. **75**(6), 2197–2210 (1996).

[5] Yuste, R., "Dendritic Spines and Distributed Circuits," Neuron **71**(5), 772–781 (2011).

[6] Sala, C. and Segal, M., "Dendritic Spines: The Locus of Structural and Functional Plasticity," Physiol. Rev. **94**(1), 141–188 (2014).

[7] Matsuzaki, M., Honkura, N., Ellis-Davies, G. C. R. and Kasai, H., "Structural basis of long-term potentiation in single dendritic spines," Nature **429**(6993), 761–766 (2004).

[8] Oh, W. C., Hill, T. C. and Zito, K., "Synapse-specific and size-dependent mechanisms of spine structural plasticity accompanying synaptic weakening.," Proc. Natl. Acad. Sci. U. S. A. **110**(4), E305-12 (2013).

[9] Tønnesen, J., Katona, G., Rózsa, B. and Nägerl, U. V., "Spine neck plasticity regulates compartmentalization of synapses," Nat. Neurosci. **17**(5), 678–685 (2014).

[10] Yuste, R. and Bonhoeffer, T., "Morphological Changes in Dendritic Spines Associated with Long-Term Synaptic Plasticity," Annu. Rev. Neurosci. **24**(1), 1071–1089 (2001).

[11] Holtmaat, A. and Svoboda, K., "Experience-dependent structural synaptic plasticity in the mammalian brain," Nat. Rev. Neurosci. **10**(9), 647–658 (2009).

[12] Matsuzaki, M., Ellis-Davies, G. C. R., Nemoto, T., Miyashita, Y., Iino, M. and Kasai, H., "Dendritic spine geometry is critical for AMPA receptor expression in hippocampal CA1 pyramidal neurons," Nat. Neurosci. **4**(11), 1086–1092 (2001).

[13] Nusser, Z., Lujan, R., Laube, G., Roberts, J. D. B., Molnar, E. and Somogyi, P., "Cell Type and Pathway Dependence of Synaptic AMPA Receptor Number and Variability in the Hippocampus," Neuron **21**(3), 545–559

(1998).
[14] Caroni, P., Donato, F. and Muller, D., "Structural plasticity upon learning: regulation and functions," Nat. Rev. Neurosci. **13**(7), 478–490 (2012).
[15] Kasai, H., Matsuzaki, M., Noguchi, J., Yasumatsu, N. and Nakahara, H., "Structure–stability–function relationships of dendritic spines," Trends Neurosci. **26**(7), 360–368 (2003).
[16] Kasai, H., Fukuda, M., Watanabe, S., Hayashi-Takagi, A. and Noguchi, J., "Structural dynamics of dendritic spines in memory and cognition," Trends Neurosci. **33**(3), 121–129 (2010).
[17] Araya, R., Vogels, T. P. and Yuste, R., "Activity-dependent dendritic spine neck changes are correlated with synaptic strength.," Proc. Natl. Acad. Sci. U. S. A. **111**(28), E2895-904 (2014).
[18] Chen, C.-C., Lu, J. and Zuo, Y., "Spatiotemporal dynamics of dendritic spines in the living brain.," Front. Neuroanat. **8**, 28 (2014).
[19] Mishchenko, Y., Hu, T., Spacek, J., Mendenhall, J., Harris, K. M. and Chklovskii, D. B., "Ultrastructural Analysis of Hippocampal Neuropil from the Connectomics Perspective," Neuron **67**(6), 1009–1020 (2010).
[20] Mukai, H., Hatanaka, Y., Mitsuhashi, K., Hojo, Y., Komatsuzaki, Y., Sato, R., Murakami, G., Kimoto, T. and Kawato, S., "Automated Analysis of Spines from Confocal Laser Microscopy Images: Application to the Discrimination of Androgen and Estrogen Effects on Spinogenesis," Cereb. Cortex **21**(12), 2704–2711 (2011).
[21] SON, J., SONG, S., LEE, S., CHANG, S. and KIM, M., "Morphological change tracking of dendritic spines based on structural features," J. Microsc. **241**(3), 261–272 (2011).
[22] Mancuso, J. J., Chen, Y., Li, X., Xue, Z. and Wong, S. T. C., "Methods of dendritic spine detection: From Golgi to high-resolution optical imaging," Neuroscience **251**, 129–140 (2013).
[23] Rochefort, N. L. and Konnerth, A., "Dendritic spines: from structure to in vivo function.," EMBO Rep. **13**(8), 699–708 (2012).
[24] Wong, S. T. C., Chen, X. and Xu, X., "Methods and systems for the analysis of 3d microscopic neuron images" (2006).
[25] "System and method for determining neuronal morphology and effect of substances thereon.", (2001).
[26] Ruszczycki, B., Szepesi, Z., Wilczynski, G. M., Bijata, M., Kalita, K., Kaczmarek, L. and Wlodarczyk, J., "Sampling issues in quantitative analysis of dendritic spines morphology," BMC Bioinformatics **13**(1), 213 (2012).
[27] Flash, F. O. R. A., Controller, M., Valley, E. and Group, L. A. W., "Method and a system for processing an image comprising dendritic spines" (2009).
[28] Basu, S., Plewczynski, D., Saha, S., Roszkowska, M., Magnowska, M., Baczynska, E. and Wlodarczyk, J., "2dSpAn: semiautomated 2-d segmentation, classification and analysis of hippocampal dendritic spine plasticity," Bioinformatics, btw172 (2016).
[29] R, W. T. and F., "4D tracking with Imaris," Bitpl. - Oxford Instruments.
[30] Swanger, S. A., Yao, X., Gross, C. and Bassell, G. J., "Automated 4D analysis of dendritic spine morphology: applications to stimulus-induced spine remodeling and pharmacological rescue in a disease model," Mol. Brain **4**(1), 38 (2011).
[31] Basu, S., Hoffman, E. and Saha, P. K., "Multi-scale Opening–A New Morphological Operator," [Image Analysis and Processing—ICIAP 2015], Springer, 417–427 (2015).
[32] Saha, P. K., Basu, S. and Hoffman, E. A., "Multiscale Opening of Conjoined Fuzzy Objects: Theory and Applications," IEEE Trans. Fuzzy Syst. **24**(5), 1121–1133 (2016).
[33] Basu, S., Raghavan, M. L., Hoffman, E. A. and Saha, P. K., "Multi-scale opening of conjoined structures with shared intensities: methods and applications," Intell. Comput. Bio-Medical Instrum. (ICBMI), 2011 Int. Conf., 128–131, IEEE (2011).
[34] Saha, P. K., Wehrli, F. W. and Gomberg, B. R., "Fuzzy Distance Transform: Theory, Algorithms, and Applications," Comput. Vis. Image Underst. **86**(3), 171–190 (2002).
[35] Saha, P. K., Udupa, J. K. and Odhner, D., "Scale-Based Fuzzy Connected Image Segmentation: Theory, Algorithms, and Validation," Comput. Vis. Image Underst. **77**(2), 145–174 (2000).
[36] Udupa, J. K. and Saha, P. K., "Fuzzy connectedness and image segmentation," Proc. IEEE **91**(10), 1649–1669 (2003).
[37] Saha, P. K. and Udupa, J. K., "Iterative relative fuzzy connectedness and object definition: theory, algorithms, and applications in image segmentation," Math. Methods Biomed. Image Anal. 2000. Proceedings. IEEE Work., 28–35, IEEE (2000).
[38] Ciesielski, K. C., Udupa, J. K., Saha, P. K. and Zhuge, Y., "Iterative relative fuzzy connectedness for multiple

objects with multiple seeds," Comput. Vis. Image Underst. **107**(3), 160–182 (2007).
[39] Guha, I., Das, N., Rakshit, P., Nasipuri, M., Saha, P. K. and Basu, S., "Design of Cerebrovascular Phantoms Using Fuzzy Distance Transform-based Geodesic Paths," Springer, Singapore, 359–367 (2018).
[40] Guha, I., Das, N., Rakshit, P., Nasipuri, M., Saha, P. K. and Basu, S., "A semiautomatic approach for segmentation of carotid vasculature from patients' CTA images," Innov. Syst. Softw. Eng. **13**(4), 243–250 (2017).
[41] Borgefors, G., "Distance transformations in digital images," Comput. vision, Graph. image Process. **34**(3), 344–371 (1986).
[42] Saha, P. K., Strand, R. and Borgefors, G., "Digital Topology and Geometry in Medical Imaging: A Survey," IEEE Trans. Med. Imaging **34**(9), 1940–1964 (2015).
[43] Schindelin, J., Arganda-Carreras, I., Frise, E., Kaynig, V., Longair, M., Pietzsch, T., Preibisch, S., Rueden, C., Saalfeld, S., Schmid, B., Tinevez, J.-Y., White, D. J., Hartenstein, V., Eliceiri, K., Tomancak, P. and Cardona, A., "Fiji: an open-source platform for biological-image analysis," Nat. Methods **9**(7), 676–682 (2012).
[44] Yushkevich, P. A., Piven, J., Hazlett, H. C., Smith, R. G., Ho, S., Gee, J. C. and Gerig, G., "User-guided 3D active contour segmentation of anatomical structures: significantly improved efficiency and reliability," Neuroimage **31**(3), 1116–1128 (2006).
[45] Worbs, T. and Förster, R., "4D-Tracking with Imaris," Bitpl. - Oxford Instruments (2007).
[46] Szepesi, Z., Hosy, E., Ruszczycki, B., Bijata, M., Pyskaty, M., Bikbaev, A., Heine, M., Choquet, D., Kaczmarek, L. and Wlodarczyk, J., "Synaptically Released Matrix Metalloproteinase Activity in Control of Structural Plasticity and the Cell Surface Distribution of GluA1-AMPA Receptors.," PLoS One **9**(5), e98274 (2014).
[47] Magnowska, M., Gorkiewicz, T., Suska, A., Wawrzyniak, M., Rutkowska-Wlodarczyk, I., Kaczmarek, L. and Wlodarczyk, J., "Transient ECM protease activity promotes synaptic plasticity," Sci. Rep. **6** (2016).